

Computational prediction of samarium hydride at megabar pressure

Zelong Zhao,¹ Siyu Chen,² Bartomeu Monserrat,^{2,3} Evgeny Plekhanov,^{1,*} and Cedric Weber^{1,†}

¹*Theory and Simulation of Condensed Matter(TSCM),
King's College London, The Strand,London WC2R 2LS,UK*
²*TCM Group, Cavendish Laboratory, University of Cambridge,
J. J. Thomson Avenue, Cambridge CB3 0HE, United Kingdom*

³*Department of Materials Science and Metallurgy, University of Cambridge,
27 Charles Babbage Road, Cambridge CB3 0FS, United Kingdom*

Samarium hydrides, belonging to the broad class of lanthanide polyhydrides, have yet to be experimentally tested at high pressure. In this study, we use random structure searches to explore multiple possible stoichiometries and propose SmH_2 with a layered hexagonal structure in the $P6/mmm$ space group and SmH_6 with hydrogen clathrate structures in the $Im\bar{3}m$ space group as theoretically stable phases of samarium hydrides at a wide range of pressures centered around 200 GPa. We further combine the first-principles methods of density functional theory and dynamical mean-field theory to explore many-body correlations in samarium hydrides, reporting electron and phonon dispersions and densities of states, and also evaluate the electron-phonon driven superconductivity to investigate low critical temperatures at 200 GPa.

I. INTRODUCTION

Superconductivity was first observed in the early 20th century at very low temperatures. Scientists have since embarked on a long-standing quest to discover materials with high critical temperatures T_c for practical use. Two mechanisms have been suggested to account for superconductivity: (i) the early proposal of Bardeen-Cooper-Schrieffer [1] in which electrons pair via phonon-mediated interactions, and (ii) spin fluctuations, which account for so-called high- T_c materials such as the copper oxides [2].

Ashcroft suggested that phonon-mediated superconductors could achieve a high T_c provided that the electron-phonon coupling strength was large [3]. The initial suggestion was to use high pressure metallic hydrogen [3], predicted to have a T_c higher than room temperature [4]. However, the pressure required to metallize hydrogen exceeds 400 GPa, which makes experiments extremely challenging [5]. Ashcroft later suggested that combining hydrogen with other elements would provide additional chemical pressure [6], resulting in a reduction of the metallization pressure while maintaining favorable phonon and electron-phonon coupling strengths. First principles calculations have successfully predicted a range of high pressure high temperature superconducting hydrides [7–9], and some of these have been experimentally observed at viable pressures and confirmed to be phonon-mediated [10–12].

There are a large number of possible candidates for high pressure hydrides, with a wide range of chemical compositions and different stoichiometries, symmetries, and lattice structures. Amongst all these possibilities, lanthanum hydride [11] has become one of the most studied compounds due to its high T_c of about 250 K at

170 GPa. The discovery of high temperature superconductivity in lanthanum hydride has motivated studies of many other lanthanide hydrides [13], both experimentally [11] and computationally [9, 14]. Despite these advances, a key lanthanide hydride, namely samarium hydride, has so far received little attention. Experimentally, samarium hydride has only been studied at ambient pressure [15], while computational studies of samarium hydride under high pressure are still lacking.

Crystal structure prediction methods[16–18] have been tremendously successful at identifying the stable phases of high pressure compounds. In these methods, first-principles calculations, typically using density functional theory (DFT), are performed across a wide range of candidate structures and compositions, and the best candidate materials are those with the lowest enthalpy. In this study, we use the *ab initio* random structure search (AIRSS) methodology [18, 19] together with DFT as implemented in the plane wave code CASTEP [20] to predict candidate structures for samarium-hydrogen compounds. The accuracy of the enthalpy determined for each generated structure depends on the quantum solver used, and we use DFT+U [21] to describe the local correlations in Sm. We search across the stoichiometry range Sm_yH_x , with $x = 1 - 18$ and $y = 1 - 2$ and under external pressures ranging from 1 to 400 GPa, as summarized in Fig. A1. Focusing on the 200 GPa results, we identify SmH_2 in the $P6/mmm$ space group and SmH_6 in the $Im\bar{3}m$ space group as stable structures, and study their electron and phonon bands and explore their potential superconductivity. We find that SmH_2 has a very low superconducting critical temperature $T_c < 1$ K and SmH_6 has a relatively higher T_c above 15 K. We also explore the role of electronic correlation in Sm hydrides using DFT augmented with dynamical mean field theory, finding correlation effects at varying degrees exhibit no noticeable impact on the electronic structure of the $P6/mmm$ phase; however, they substantially influence the $Im\bar{3}m$ phase.

* evgeny.plekhanov@kcl.ac.uk

† cedric.weber@kcl.ac.uk

II. METHODOLOGY

A. Theoretical background

1. Electronic structure methods

Within DFT [22, 23] the many-body Schrödinger equation is solved by mapping the problem onto an auxiliary one-body problem with the same electronic density as the many-body system. This auxiliary Kohn-Sham (KS) system obeys:

$$\left[-\frac{\hbar^2}{2m} \nabla^2 + V_{\text{eff}}(\mathbf{r}) \right] \varphi_i(\mathbf{r}) = \varepsilon_i \varphi_i(\mathbf{r}), \quad (1)$$

where the electrons experience an effective potential $V_{\text{eff}}(\mathbf{r})$:

$$V_{\text{eff}}(\mathbf{r}) = V_{\text{ext}}(\mathbf{r}) + \int \frac{n(\mathbf{r}')}{|\mathbf{r} - \mathbf{r}'|} d^3\mathbf{r}' + V_{\text{XC}}[n(\mathbf{r})]. \quad (2)$$

In these equations, $\varphi_i(\mathbf{r})$ is the i -th KS orbital, and the electronic density $n(\mathbf{r})$ is derived from the densities of the KS orbitals occupied up to the Fermi level. The accuracy of the KS scheme depends on the choice of exchange correlation (XC) functional. Commonly used approximations include the Local Density Approximation (LDA) and Generalized Gradient Approximations (GGA). In this work, we adopt the Perdew-Burke-Ernzerhof (PBE) XC functional [24], which is a type of GGA.

The amount of correlations contained in the DFT XC functional is not sufficient to treat the strong Coulomb repulsion in partially filled d and f orbitals. Within standard approximations to DFT functionals, these strongly correlated orbitals appear to be excessively delocalized. This lack of localization can be, to some extent, corrected with the DFT+U scheme, where the DFT energy functional is combined with an additional term proportional to a parameter, called Hubbard U , which penalizes the configurations with doubly occupied orbitals [25].

A higher level treatment of the strong Coulomb repulsion is provided by the DFT + Dynamical Mean Field Theory (DFT+DMFT) approach [26–28], where the temporal correlations are taken into account exactly, while the treatment of the spatial correlations becomes exact in the limit of infinite coordination of the correlated orbitals. Within DFT+DMFT, the system of correlated orbitals (usually d or f , or a subset of them) connected to a chemical environment is mapped onto an auxiliary problem of an Anderson impurity connected to a bath of uncorrelated orbitals. The latter problem is then solved either numerically (e.g. quantum Monte Carlo, exact diagonalization) or analytically by using some approximation (e.g. Hubbard-I, auxiliary bosons). The results of such an impurity problem are then mapped back onto the original correlated lattice problem. The details of the DFT+DMFT implementation used in the present work can be found in Refs. 28 and 29.

2. Structure searching

We perform structure searches using AIRSS [18, 19] together with the DFT+U methodology. The efficiency of the structure search is crucial for searching low enthalpy compounds, and we adopt several strategies to accelerate calculations, including the adjustment of the volume and the use of low-resolution calculations during the initial potential energy surface scan, followed by higher-precision calculations. To obtain the convex hull of samarium hydride, we calculate the enthalpy of formation with:

$$\Delta H = H_{\text{Sm}_y\text{H}_x} - x H_{\text{H}} - y H_{\text{Sm}}. \quad (3)$$

This formula requires the knowledge of stable phases of the end members samarium [30] and hydrogen [31] atoms, which we take from the literature. For example, at 200 GPa, hydrogen is in a phase of $C2/c$ symmetry and samarium is in the $oF8$ phase.

We highlight that it is generally impossible to confirm whether the global enthalpy minimum has been found due to the exponential scaling cost of searching over the potential energy landscape. However, over the past decade structure searching methods have been shown to provide important insights into high pressure phases and often predicted the correct structures subsequently identified experimentally.

B. Computational details

In the present work, we perform the first principles calculations using the CASTEP and QUANTUM ESPRESSO codes. We use the Perdew-Burke-Ernzerhof (PBE) exchange-correlation function together with ultra-soft pseudopotentials for Sm [Xe]4f⁶6s² and H 1s¹.

We perform a random structure search over the samarium-hydrogen binary combining AIRSS [18] and CASTEP [20]. We adopt a two-step approach to facilitate the random structure search with DFT+U: (1) we explore different stoichiometries using a coarse Monkhorst-Pack (MP) \mathbf{k} -point grid ($2\pi \times 0.03 \text{ \AA}^{-1}$), a kinetic energy cut-off of $E_{\text{cut}} = 500 \text{ eV}$, a force tolerance of 0.05 eV/\AA ; and (2) we perform additional calculations on a small subset of structures having the lowest enthalpy with a denser MP \mathbf{k} -point grid ($2\pi \times 0.01 \text{ \AA}^{-1}$), $E_{\text{cut}} = 750 \text{ eV}$, force tolerance 0.001 eV/\AA , and $U = 6 \text{ eV}$ (Fig. A2). We note that the parameter set used in the second step ensures that the overall energy precision is within 1 meV/atom (see Fig. A3, Fig. A4).

For the pressure of 200 GPa, we also perform DFT+DMFT calculations as implemented within CASTEP [20, 28, 29] using the same DFT parameters as the ones used in step (2) of the searches. Additionally, these calculations used a Hubbard $U = 6 \text{ eV}$ and an additional Hund's coupling $J = 0.855 \text{ eV}$ [32].

We calculate phonon dispersions in the harmonic approximation via the finite difference method [33] combined with nondiagonal supercells [34]. The 3-dimensional Farey \mathbf{q} -grid of order 6 is used for careful sampling of the dynamical matrices [35] and confirming the dynamical stability of the systems. The electron-phonon coupling properties were computed via density functional perturbation theory (DFPT), which was implemented using the QUANTUM ESPRESSO package as described by Giannozzi et al. [36]. The uniform \mathbf{q} -point grids used to sample the Brillouin zone are of size $6 \times 6 \times 6$. The DFT settings involved in the DFPT calculation were identical to those used in step (2) of the searches. The superconducting critical temperature was found using the Allen and Dynes [37] revised McMillan [38] equation.

III. RESULT AND DISCUSSION

A. Structure Search

The results of the random structure search are summarized by the convex hull shown in Fig. 1. Each point corresponds to a distinct structure at a certain pressure and stoichiometry. In the convex Hull, the horizontal axis is the ratio x of hydrogen atoms relative to the total number of atoms in the cell in one formula unit (f.u.). The left side, corresponding to $x = 0$, is the samarium bulk, and the right side, corresponding to $x = 1$, is the hydrogen bulk. The solid line connects thermodynamically stable phases.

Figure 1 indicates that there are two stable structure in the samarium-hydrogen system at 200 GPa, one with stoichiometry SmH_2 and space group $P6/mmm$, and another with stoichiometry SmH_6 and space group $Im\bar{3}m$. Interestingly, the SmH_2 and SmH_6 structure are highly symmetric, a feature also observed in other high-pressure lanthanide hydride systems, and is analogous to the ScH_2 phase obtained in [9] for the scandium-hydrogen system. The SmH_6 structure is analogous to YH_6 in [39].

Overall, the lowest enthalpy structures tend to possess a high symmetry at high pressure. It is important to note that the higher precision calculations on the most stable structures identified during the searches do not change the overall ranking of the low-enthalpy phases (see Fig. A2). Specifically, SmH_2 in the $P6/mmm$ and SmH_6 in the $Im\bar{3}m$ space group remains the most stable phase.

We also remark that the enthalpies of elemental hydrogen and samarium enter the calculation of the formation energy. In this work, we use the theoretical estimates of solid hydrogen from Ref. [31], and the $oF8$ structure of samarium reported in Ref. [30]. Furthermore, our results remain unchanged upon a reasonable variation of the estimated hydrogen enthalpy, and in particular the order of the obtained phases remains the same in Fig. 1.

Between pressures of 50 GPa and 100 GPa, the most stable stoichiometries are SmH_2 and SmH_4 (as shown in

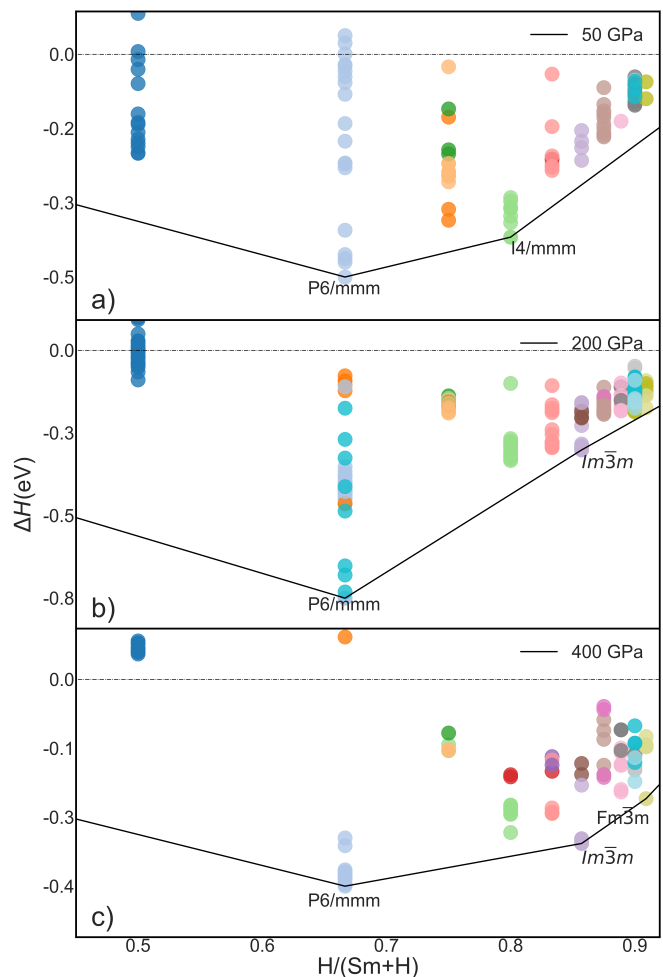


FIG. 1. Maxwell convex hull reported at 50, 200, and 400 GPa. The solid line connects stable phases and the dashed line connects the lowest enthalpy phases at each stoichiometry (not necessarily stable). The end members are hydrogen in the $C2/c$ structure [31] and samarium in the $oF8$ phase [30].

Fig. 2). SmH_2 has a layered structure that is similar to MgB_2 , while SmH_4 has an $I4/mmm$ structure that has also been observed as a stable phase at lower pressures (Ref.,[9]). However, the further analysis focuses only on the pressure of 200 GPa, which is a typical pressure range used in high pressure hydride experiments.

We also note that the Sm-H convex Hull was previously reported in Ref. [9]. However, this report exclude a structure search of the Sm-H system; instead structure searches were performed for other lanthanide-hydrogen systems, the lanthanide elements were replaced by Sm in the final structures. Of the Sm-H structures reported in Ref. [9], have rediscovered the $Im\bar{3}m$, $I4/mmm$ and $Fm\bar{3}m$ in our searches, and identified for the first time the stable SmH_2 $P6/mmm$ phase. Our results are also consistent with the observation in Ref. [9] that hydrogen-rich phases become competitive at higher pressures.

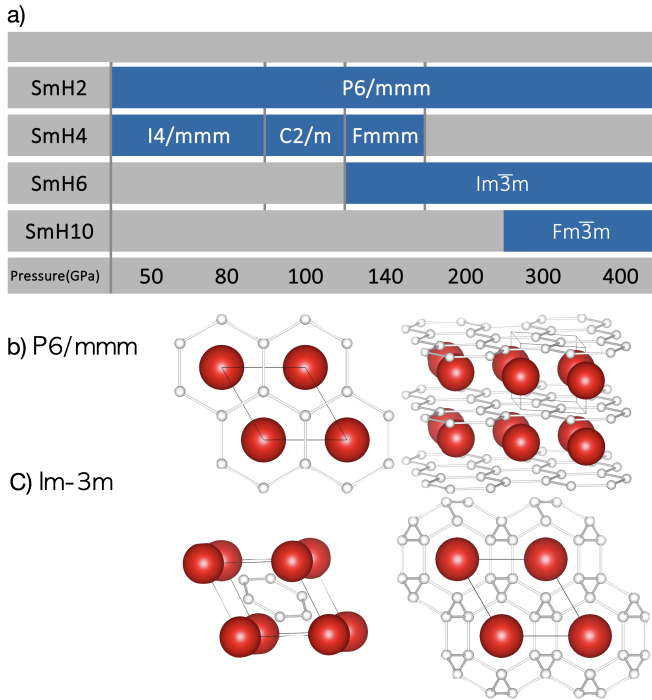


FIG. 2. (a) Stable phase of Sm. $P6/mmm$ is a stable phase for all range of pressure. Other stable phase tends to have more hydrogen as pressure increases. (b) $P6/mmm$ of SmH_2 and (c) $Im\bar{3}m$ of SmH_6 at 200 GPa.

B. Electronic properties of SmH_2 $P6/mmm$ and SmH_6 $Im\bar{3}m$

To investigate the electronic properties of the SmH_2 $P6/mmm$ and SmH_6 $Im\bar{3}m$ phase, we calculate the corresponding partial density of states (PDOS). Only samarium contributes f electrons, and TOT indicates the total DOS of SmH_2 . Pure DFT calculations using PBE do not apply any specialized treatment to f -orbital electrons. As a result, the electronic structures of $P6/mmm$ (Fig. 3 a)) and $Im\bar{3}m$ (Fig. 4 a)) are primarily dominated by f -orbital electrons. The Hubbard U term in the DFT+ U method includes the Mott transition via splitting the DOS of correlated orbitals and pushing the density of state peak away from the Fermi level.

To further explore the correlation effects of f electrons, we perform DFT+DMFT calculations for SmH_2 $P6/mmm$ and SmH_6 $Im\bar{3}m$ at 200 GPa. We employed charge self-consistent (CSC) DFT+DMFT, which signifies the convergence between the chemical potential involved in the DMFT calculation and the charge density obtained from the self-consistent field (SCF) calculation. Our calculations show that the chemical potentials of DFT+ U and DFT+DMFT show similar densities of states near the Fermi level.

The phonon dispersions of SmH_2 $P6/mmm$ and SmH_6 $Im\bar{3}m$ at 200 GPa using DFT and DFT+ U exhibit no soft modes, which indicates that the predicted phases

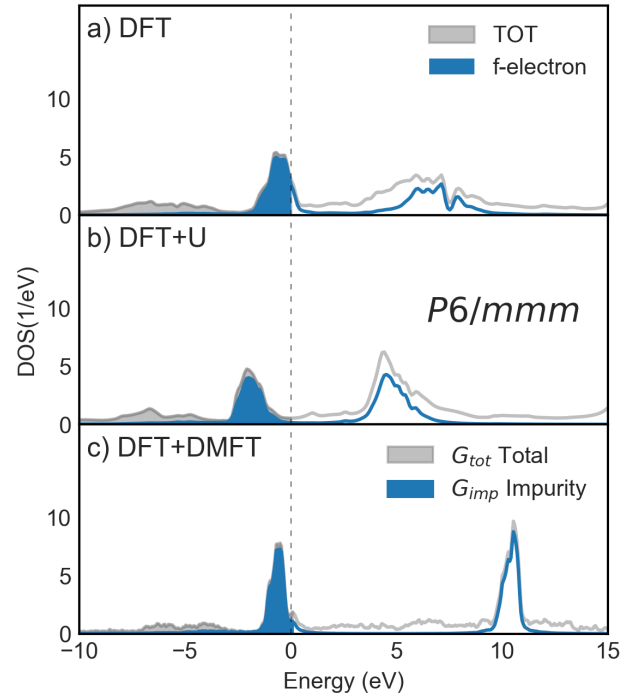


FIG. 3. DOS for SmH_2 $P6/mmm$ as predicted by (a) DFT and (b) DFT+ U with $U=6$ eV. (c) Spectral function calculated using DFT+DMFT, incorporating a Hubbard U of 6 eV and Hund's coupling $J=0.85$ eV. Here, G_{tot} represents the spectral function derived from the total Green's function, while G_{imp} indicates the spectral function obtained from the impurity Green's function.

are dynamically stable. The phonons of samarium hydride show a similar pattern to those of other lanthanide hydrides. The most prominent feature is a large gap between optical and acoustic branches arising from the large difference in mass between lanthanides and hydrogen. Interestingly, the Hubbard U term has a negligible effect on the phonon dispersion. We also highlight that different values of U lead to an equilibrium volume for the $P6/mmm$ structure that varies from $15.72(\text{\AA})^3$ to $16.09(\text{\AA})^3$ for U between 0 eV and 6 eV and for the $Im\bar{3}m$ structure that varies from $21.35(\text{\AA})^3$ to $22.45(\text{\AA})^3$. Given the negligible effect of the U value on the phonon frequencies, there is likely a competition between the volume changes and the effect of U on the force constants.

We further performed density functional perturbation theory (DFPT) calculations to estimate the electron-phonon coupling (EPC) strength and calculated the superconducting temperature (T_c) via the Allen and Dynes [37] revised McMillan [38] equation:

$$T_c = \frac{\omega_{\log}}{1.2} \exp \left[\frac{-1.04(1 + \lambda)}{\lambda(1 - 0.62\mu^*) - \mu^*} \right] \quad (4)$$

In this expression, μ^* is the Coulomb potential with typical values between 0.1 and 0.15, λ is the electron-phonon

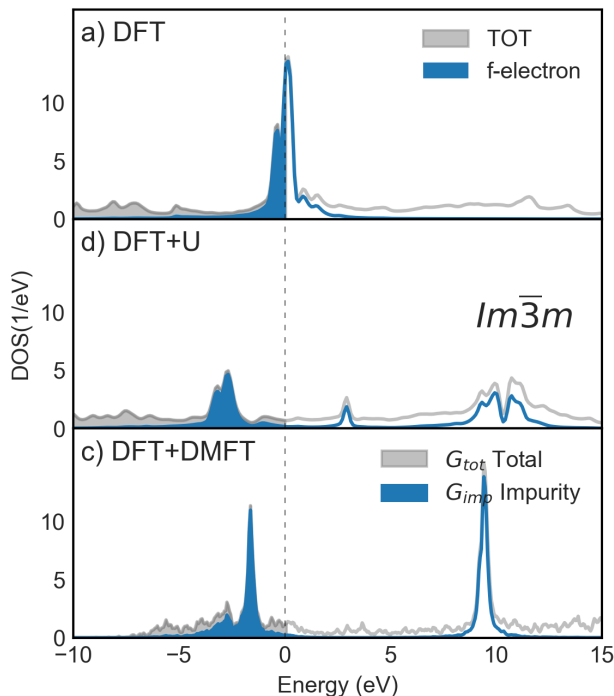


FIG. 4. DOS for SmH_6 $Im\bar{3}m$ as predicted by (a) DFT with $U=0$ eV and (b) DFT+U with $U=6$ eV. (c) Spectral function calculated using DFT+DMFT.

TABLE I. Electron-phonon coupling

	λ	ω_{\log}	$T_c(K)$
$P6/mmm$	0.28	357.69	0.10 (K) ($\mu^* = 0.10$)
			0.00 (K) ($\mu^* = 0.15$)
$Im\bar{3}m$	0.65	900.04	26.35 (K) ($\mu^* = 0.10$)
			15.50 (K) ($\mu^* = 0.15$)

coupling strength, and ω_{\log} is the logarithmic average frequency. These quantities are evaluated via integrals of the Eliashberg function.

In SmH_2 $P6/mmm$, the electron-phonon coupling is relatively low, with λ equal to 0.28, resulting in a T_c value below 1 K for μ^* ranging between 0.1 and 0.15. Conversely, the $Im\bar{3}m$ structure exhibits a higher peak at the Fermi level, leading to a comparatively elevated predicted T_c . The relatively low superconducting critical temperatures in the Sm-H system are consistent with earlier work [9, 40] which shows higher T_c for La/Y hydrides and lower T_c for intermediate series lanthanides such as Sm. The origin of the low superconducting critical temperatures in samarium hydride could be caused by the low hydrogen DOS at the Fermi level and the associated weak electron-phonon coupling strength.

In conclusion, we have used random structure searches via the AIRSS method [18, 19, 31] to explore high pressure samarium hydride, a material whose structure re-

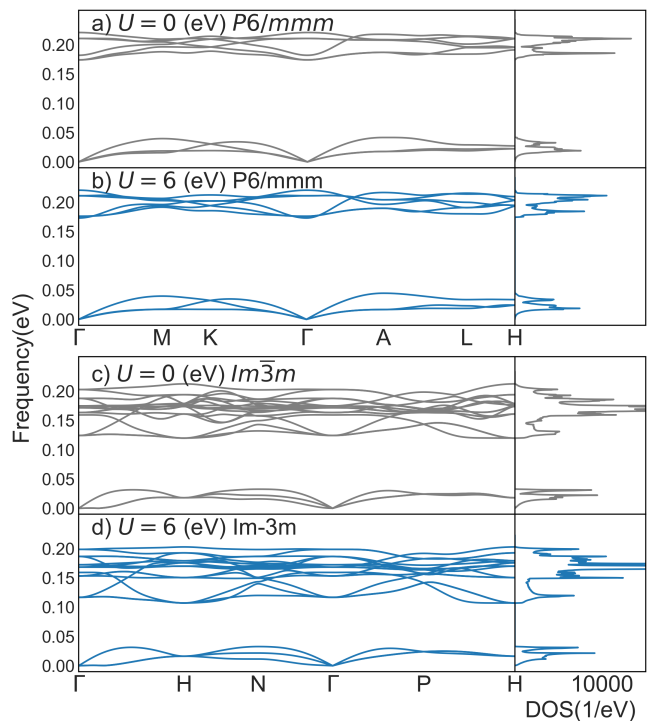


FIG. 5. The left side panel shows the SmH_2 in the $P6/mmm$ and SmH_6 in the $Im\bar{3}m$ space group phonon dispersion and the right side panel shows the phonon DOS. Both are calculated with a coarse q-point grid size of $6 \times 6 \times 6$. Electronic method is DFT+U with U as indicated.

mains unknown experimentally at high pressures. Focusing on a pressure of 200 GPa, we predicted that SmH_2 with a structure of $P6/mmm$ and SmH_6 with a structure of $Im\bar{3}m$ are the stable phase. Other Stable phases are found for SmH_y for y equal to 4 and 10. These results indicate that high pressure samarium hydride compounds could be hydrogen-rich. We have conducted a comprehensive analysis of the electronic structure and lattice dynamics of SmH_2 and SmH_6 at 200 GPa. Our findings reveal that both SmH_2 and SmH_6 exhibit dynamic stability for the investigated U of 6 eV. Additionally, we determined that the T_c of SmH_2 is below 1 K, while the T_c of SmH_6 falls within the range of 15 to 26 K.

This work opens new avenues for studying hydrides at high pressure. As shown in this work, new highly symmetric phases of correlated matter can emerge, leading to a breadth of properties which are interesting for possible applications, such as superconductivity. The method used in this work is quite general and can be extended to other systems of interest.

ACKNOWLEDGEMENTS

C.W. and E.P. are supported by the grant [EP/R02992X/1] from the UK Engineering and Physi-

cal Sciences Research Council (EPSRC). S.C. acknowledges financial support from the Cambridge Trust and from the Winton Programme for the Physics of Sustainability. B.M. acknowledges support from a UKRI Future Leaders Fellowship (Grant No. MR/V023926/1), from the Gianna Angelopoulos Programme for Science, Technology, and Innovation, and from the Winton Programme for the Physics of Sustainability. This work was performed using resources provided by the ARCHER

UK National Supercomputing Service and the Cambridge Service for Data Driven Discovery (CSD3) operated by the University of Cambridge Research Computing Service (www.csd3.cam.ac.uk), provided by Dell EMC and Intel using Tier-2 funding from the Engineering and Physical Sciences Research Council (capital grant EP/P020259/1), and DiRAC funding from the Science and Technology Facilities Council (www.dirac.ac.uk).

-
- [1] J. Bardeen, L. N. Cooper, and J. R. Schrieffer, *Physical review* **108**, 1175 (1957).
- [2] V. L. Ginzburg, V. L. Ginzburg, and L. Landau, *On the theory of superconductivity* (Springer, 2009).
- [3] N. W. Ashcroft, *Physical Review Letters* **21**, 1748 (1968).
- [4] J. M. McMahon and D. M. Ceperley, *Physical Review B* **84**, 144515 (2011).
- [5] R. P. Dias and I. F. Silvera, *Science* **355**, 715 (2017).
- [6] N. Ashcroft, *Physical Review Letters* **92**, 187002 (2004).
- [7] D. Duan, Y. Liu, F. Tian, D. Li, X. Huang, Z. Zhao, H. Yu, B. Liu, W. Tian, and T. Cui, *Scientific reports* **4**, 6968 (2014).
- [8] H. Liu, I. I. Naumov, R. Hoffmann, N. Ashcroft, and R. J. Hemley, *Proceedings of the National Academy of Sciences* **114**, 6990 (2017).
- [9] F. Peng, Y. Sun, C. J. Pickard, R. J. Needs, Q. Wu, and Y. Ma, *Physical review letters* **119**, 107001 (2017).
- [10] A. Drozdov, M. Erements, I. Troyan, V. Ksenofontov, and S. I. Shylin, *Nature* **525**, 73 (2015).
- [11] M. Somayazulu, M. Ahart, A. K. Mishra, Z. M. Geballe, M. Baldini, Y. Meng, V. V. Struzhkin, and R. J. Hemley, *Physical Review Letters* **122**, 027001 (2019).
- [12] A. Drozdov, P. Kong, V. Minkov, S. Besedin, M. Kuzovnikov, S. Mozaffari, L. Balicas, F. Balakirev, D. Graf, V. Prakapenka, *et al.*, *Nature* **569**, 528 (2019).
- [13] Y. Fukai, *The metal-hydrogen system: basic bulk properties*, Vol. 21 (Springer Science & Business Media, 2006).
- [14] E. Plekhanov, Z. Zhao, F. Macheda, Y. Wei, N. Bonini, and C. Weber, *Physical Review Research* **4**, 013248 (2022).
- [15] J. Daou, P. Vajda, and J. Burger, *Solid state communications* **71**, 1145 (1989).
- [16] C. W. Glass, A. R. Oganov, and N. Hansen, *Computer physics communications* **175**, 713 (2006).
- [17] Y. Wang, J. Lv, L. Zhu, and Y. Ma, *Computer Physics Communications* **183**, 2063 (2012).
- [18] C. J. Pickard and R. Needs, *Journal of Physics: Condensed Matter* **23**, 053201 (2011).
- [19] C. J. Pickard and R. Needs, *Physical Review Letters* **97**, 045504 (2006).
- [20] S. J. Clark, M. D. Segall, C. J. Pickard, P. J. Hasnip, M. I. Probert, K. Refson, and M. C. Payne, *Zeitschrift für kristallographie-crystalline materials* **220**, 567 (2005).
- [21] M. Cococcioni, *Correlated Electrons: From Models to Materials Modeling and Simulation* **2** (2012).
- [22] W. Kohn and L. J. Sham, *Physical review* **140**, A1133 (1965).
- [23] P. Hohenberg and W. Kohn, *Physical review* **136**, B864 (1964).
- [24] J. P. Perdew, K. Burke, and M. Ernzerhof, *Physical review letters* **77**, 3865 (1996).
- [25] B. Himmetoglu, A. Floris, S. De Gironcoli, and M. Cococcioni, *International Journal of Quantum Chemistry* **114**, 14 (2014).
- [26] A. Georges, G. Kotliar, W. Krauth, and M. J. Rozenberg, *Reviews of Modern Physics* **68**, 13 (1996).
- [27] G. Kotliar, S. Y. Savrasov, K. Haule, V. S. Oudovenko, O. Parcollet, and C. Marianetti, *Reviews of Modern Physics* **78**, 865 (2006).
- [28] E. Plekhanov, P. Hasnip, V. Sacksteder, M. Probert, S. J. Clark, K. Refson, and C. Weber, *Physical Review B* **98**, 075129 (2018).
- [29] E. Plekhanov, N. Bonini, and C. Weber, *Phys. Rev. B* **104**, 235131 (2021).
- [30] S. Finnegan, E. Pace, C. Storm, M. McMahon, S. MacLeod, H.-P. Liermann, and K. Glazyrin, *Physical Review B* **101**, 174109 (2020).
- [31] C. J. Pickard and R. J. Needs, *Nature Physics* **3**, 473 (2007).
- [32] D. Banerjee, E. Plekhanov, I. Rungger, and C. Weber, *Physical Review B* **105**, 195135 (2022).
- [33] K. Parlinski, Z. Q. Li, and Y. Kawazoe, *Phys. Rev. Lett.* **78**, 4063 (1997).
- [34] J. H. Lloyd-Williams and B. Monserrat, *Phys. Rev. B* **92**, 184301 (2015).
- [35] S. Chen, P. T. Salzbrenner, and B. Monserrat, *Physical Review B* **106**, 155102 (2022).
- [36] P. Giannozzi, S. Baroni, N. Bonini, M. Calandra, R. Car, C. Cavazzoni, D. Ceresoli, G. L. Chiarotti, M. Cococcioni, I. Dabo, *et al.*, *Journal of physics: Condensed matter* **21**, 395502 (2009).
- [37] P. B. Allen and R. Dynes, *Physical Review B* **12**, 905 (1975).
- [38] W. McMillan, *Physical Review* **167**, 331 (1968).
- [39] P. Kong, V. S. Minkov, M. A. Kuzovnikov, A. P. Drozdov, S. P. Besedin, S. Mozaffari, L. Balicas, F. F. Balakirev, V. B. Prakapenka, S. Chariton, *et al.*, *Nature communications* **12**, 1 (2021).
- [40] D. V. Semenov, I. A. Kruglov, I. A. Savkin, A. G. Kvashnin, and A. R. Oganov, *Current Opinion in Solid State and Materials Science* **24**, 100808 (2020).

Supplemental Materials: Computational prediction of Samarium Hydride at Mgebar pressure

I. RANDOM STRUCTURE SEARCH

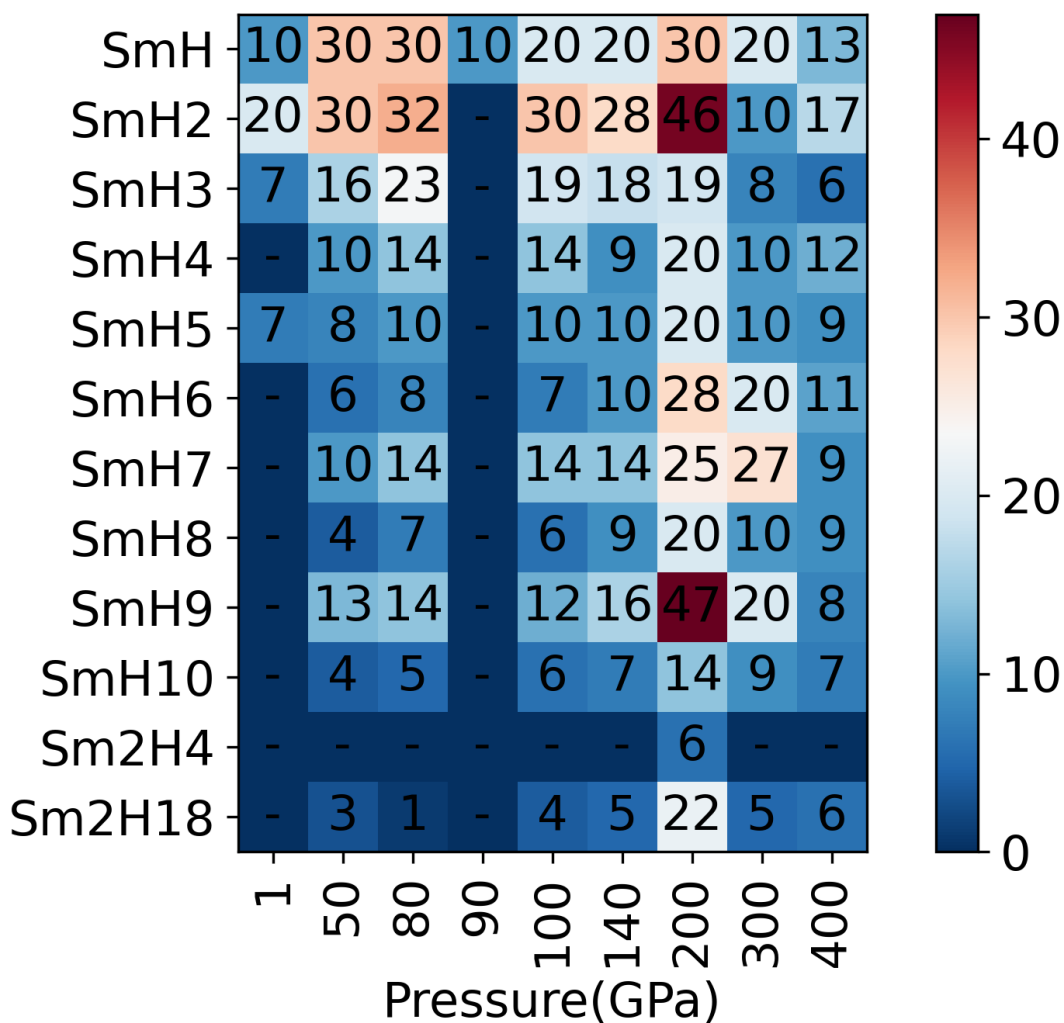


FIG. A1. Size of the phase database. Y-axis is stoichiometry of Samarium and hydrogen. X-axis is pressure we performed random structure search. Phase we searched "-" represents we did not search for this pressure and stoichiometry. The number indicated in each of the cell is the total number of distinct structure identified by AIRSS at each pressure for each stoichiometry. Colour bar blue for less search performed for this combination and red represents for more intense search.

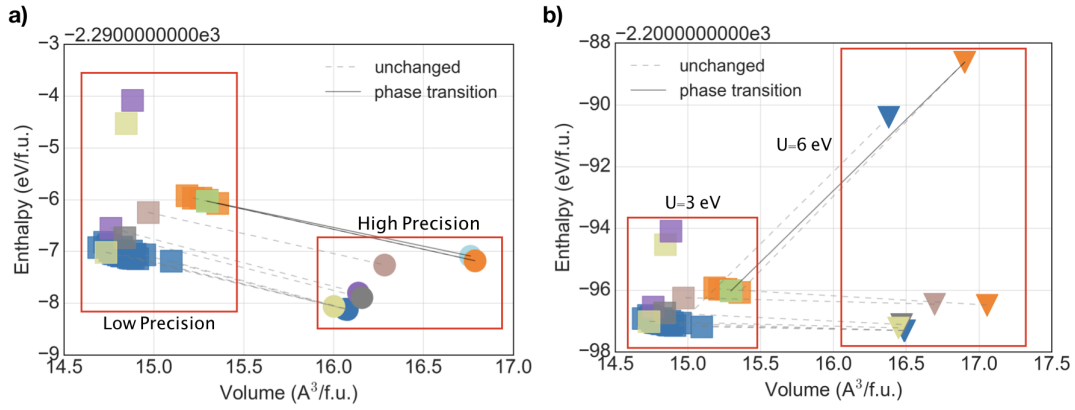


FIG. A2. AIRSS generated phases of SmH_2 at 200 GPa. Squares and circles indicate phases of SmH_2 . Color indicates space group. Square indicate relevant DFT+U settings is "step 1" as mentioned in the main paper and circles represent "step 2". X axis is volume of the unit cell and Y axis is DFT+U calculated enthalpy. Phases in both "Low Precision and (b) "U=3eV" boxes are same group of phases and DFT+U settings are indicated are "step 1" in the method section. (a) DFT settings changed between "Low Precision" ("step 1") to "High Precision" ("step 2") but Hubbard U is kept same. (b) DFT settings changed as in (a) but Hubbard U involved in DFT+U calculation changed from 3 eV to 6 eV.

TABLE A1. Lattice parameters of Sm_xH_y

	Space group	Lattice Parameters Å	Atom	Atomic fractional coordinates		
				X	Y	Z
SmH_2 (200 GPa)	$P6/mmm$	$a=b=2.692$	Sm(1b)	0.000	0.000	0.000
		$c=2.562$	H(2c)	1/3	2/3	1/2
		$\alpha = \beta = \gamma = 90^\circ$				
		$\gamma = 120^\circ$				
SmH_4 (200 GPa)	$I4/mmm$	$a=b=2.546$	Sm(2b)	0.000	0.000	1/2
		$c=5.618$	H(4e)	1/2	1/2	0.693
		$\alpha = \beta = \gamma = 90^\circ$	H(4d)	0.000	1/2	3/4
SmH_4 (100 GPa)	$C2/m$	$a=5.553$	Sm(2a)	1/2	1/2	0.000
		$b=2.842$	H(4i)	0.901	1/2	0.455
		$c=3.041$	H(4i)	0.747	1/2	0.669
		$\alpha = \gamma = 90^\circ$				
		$\beta = 112.492^\circ$				
SmH_4 (140 GPa)	$Fmmm$	$a=3.792$	Sm(4b)	0.000	0.000	1/2
		$b=4.141$	H(8f)	3/4	3/4	3/4
		$c=5.238$	H(8i)	1/2	1/2	0.073
		$\alpha = \beta = \gamma = 90^\circ$				
SmH_6 (140 GPa)	$Im\bar{3}m$	$a=b=c=3.603$	Sm(2a)	1/2	1/2	1/2
		$\alpha = \beta = \gamma = 90^\circ$	H(12d)	1/2	1/4	0.000
SmH_{10} (400 GPa)	$Fm\bar{3}m$	$a=b=c=4.434$	Sm(4a)	1/2	0.000	1/2
		$\alpha = \beta = \gamma = 90^\circ$	H(8c)	3/4	1/4	1/4
			H(32f)	0.620	0.620	0.380

II. DFT+DMFT CALIBRATION

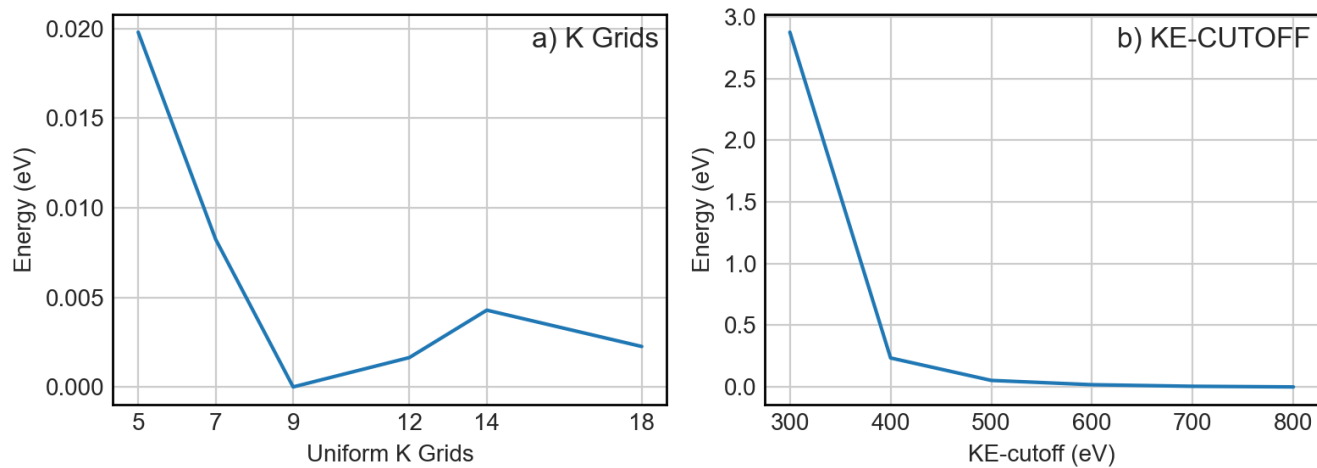


FIG. A3. DFT Convergence test of $P6/mmm$: a) K-points test. KE-cutoff 400eV with XC functional PBE. b) KE cut-off test with K-points grids $14 \times 14 \times 14$ and XC functional PBE.

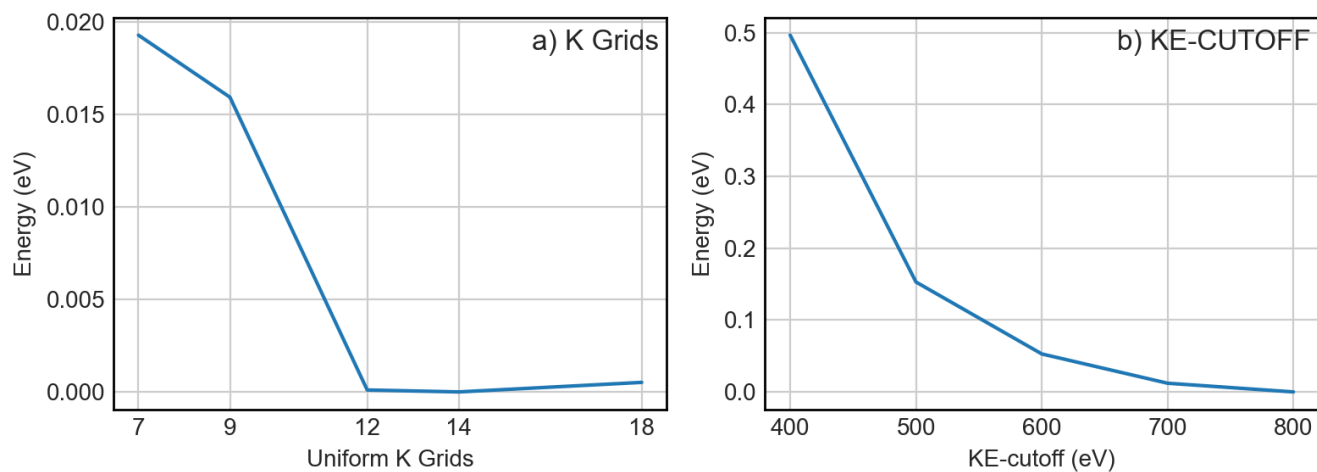


FIG. A4. DFT Convergence test of $Im\bar{3}m$: a) K-points test. KE-cutoff 400eV with XC functional PBE. b) KE cut-off test with K-points grids $14 \times 14 \times 14$ and XC functional PBE.

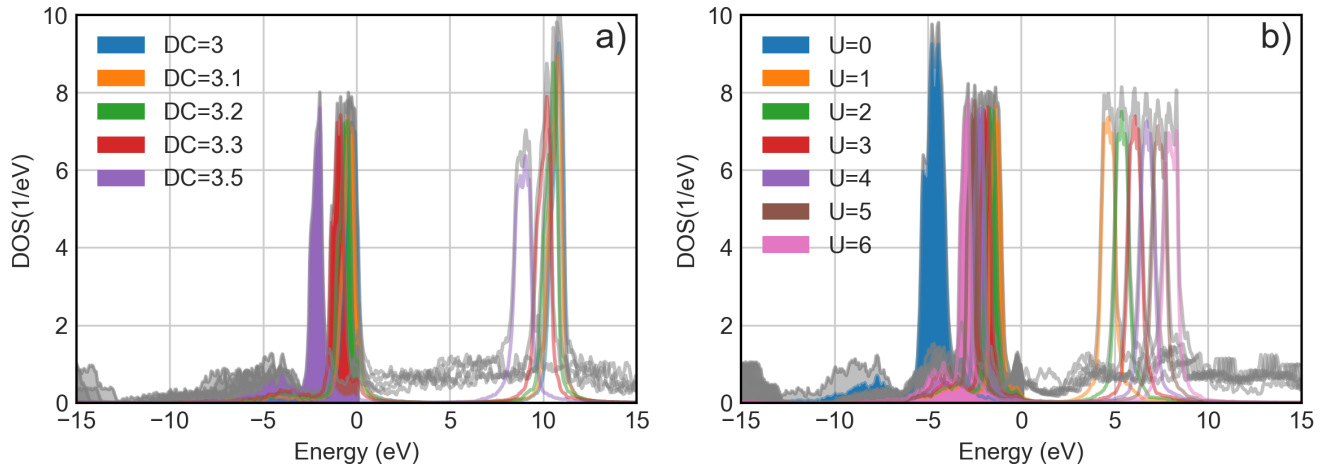


FIG. A5. (a) DC test with DFT+DMFT CSC DOS for $P6/mmm$ SmH_2 : Hubbard U equal to 6eV and Hund's coupling J equal to 0.855eV (b) Hubbard U test with 1-shot DOS for $P6/mmm$ SmH_2 : DC equal 3.5 and Hund's coupling J equal 0.855. Notice that Converged DC for $P6/mmm$ is around 3.1